Which parts of the road guide obstacle avoidance? Quantifying the driver's risk field

Kolekar, Sarvesh; de Winter, Joost; Abbink, David

DOI
10.1016/j.apergo.2020.103196

Publication date
2020

Document Version
Final published version

Published in
Applied Ergonomics

Applied Ergonomics 89 (2020) 103196

Contents lists available at ScienceDirect

Applied Ergonomics

journal homepage: http://www.elsevier.com/locate/apergo

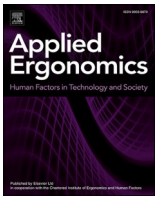

Which parts of the road guide obstacle avoidance? Quantifying the driver's risk field

Sarvesh Kolekar *, Joost de Winter, David Abbink

Department of Cognitive Robotics, Faculty of Mechanical, Maritime, and Materials Engineering (3mE), Delft University of Technology, the Netherlands

ARTICLE INFO

Keywords:
Field of safe travel
Risk
Obstacle avoidance
Potential field
Driving

ABSTRACT

Gibson and Crooks (1938) argued that a 'field of safe travel' could qualitatively explain drivers' steering behavior on straights, curved roads, and while avoiding obstacles. This study aims to quantitatively explain driver behavior while avoiding obstacles on a straight road, and quantify the 'Driver's Risk Field' (DRF). In a fixed-based driving simulator, 77 (7 longitudinal and 11 lateral) positions of the obstacles were used to quantify the subjectively perceived and objectively (maximum absolute steering angle) measured DRF for eight participants. The subjective response was a numerical answer to the question "How much steering do you think you need at this moment in time?" The results show that the propagation of the width of the DRF, along the longitudinal distance, resembled an hourglass shape, and all participants responded to obstacles that were placed beyond the width of the car. This implies that the Driver's Risk Field is wider than the car width.

1. Introduction

Many car manufacturers worldwide are developing highly automated driving systems that are expected to contribute to driver comfort and safety (Reimer, 2014). Before automated driving systems can be deployed on a widespread scale, various technological challenges still need to be resolved. One specific challenge is that current automated driving systems are conservative, strictly obedient to the traffic rules, and unable to exhibit natural driving behaviors, rendering them, at present, slow and inefficient (Neumann, 2016). A second challenge is that until fully (SAE Level 5) autonomous cars are introduced, there will be a need for automation systems that keep the human involved in the driving task. Such systems may have to interact with the driver in a human-like manner (Faltaous et al., 2018; Muslim and Itoh, 2018; Niu et al., 2018), for example via a shared control system (Abbink et al., 2012).

This need for effective interaction, and the inefficiencies of (partially and highly) automated vehicles provides an impetus for developing automated cars that drive in a human-like manner, with acceptable safety margins towards other road users and road boundaries (Kauffmann et al., 2018). At present, however, there is no generally accepted model that quantitatively captures human driving behavior (Papakostopoulos et al., 2017; Melman et al., 2018; Lappi and Mole, 2018). As early as 1970, a driver task analysis by McKnight and Adams (1970) identified over 1000 characteristics (vehicle, roadway, traffic, and environment characteristics) of the highway transportation system to which the driver must respond. The sheer complexity of driving makes it impractical to rely on separate heuristics for every driving situation, which is why it would be beneficial to identify the general principles that govern human driving behavior.

So far, attempts at identifying the underlying principles of human driving behavior have resulted in a rather fragmented understanding of the driving task, where specific visual cues are used to predict the driver's behavior in specific driving tasks (Papakostopoulos et al., 2017). For example, the optical edge rate has been used to predict the speed at which drivers drive (Denton, 1980), whereas Lee (1976) showed that time to collision (TTC) is predictive of human braking behavior while approaching a static or moving obstacle. Godthelp and colleagues provided evidence that time-to-lane-crossing (TLC) can describe the positioning of a vehicle in a lane while driving on straights and curves (Godthelp et al., 1984; Godthelp, 1986). The TLC model of Godthelp was extended by Boer, to account for the variability of lateral position (satisficing) while driving in curves (Boer, 2016). Additionally, models based on a 'potential-field' have tried to solve the path planning problem by assigning different costs to different obstacles and finding the path of least cost (Rasekhipour, 2017). However, these potential-field models have not been tested for human-likeliness.

The first attempt of creating a unified model of human driving

* Corresponding author.
E-mail addresses: s.b.kolekar@tudelft.nl, kolekar.sarvesh380@gmail.com (S. Kolekar).

https://doi.org/10.1016/j.apergo.2020.103196
Received 13 December 2018; Received in revised form 10 June 2020; Accepted 17 June 2020
Available online 21 July 2020

behavior can be found in Gibson and Crooks' 1938 paper, where they proposed the concept of 'field of safe travel' (Gibson and Crooks, 1938). They defined the field of safe travel as the "field of possible paths which the car may take unimpeded" (p. 454); it was described as comprising both subjective elements ("subjective experience of the driver", p. 455) and objective elements ("it exists objectively as the actual field within which the car can safely operate", p. 455). Gibson and Crooks illustrated the field with various drawings of driving situations (e.g., straight-line driving, curve driving, moving pedestrian, moving obstacle, overtaking a parked car, blind corner). The study, however, was qualitative and based on discussions between a psychologist and a student of driving. Thus, although the field of safe travel is introspectively plausible and highly influential, it lacks operationalization and has limited empirical validation (Smith and Källhammer, 2012).

In recent years some automated cars have been based on concepts similar to that of Gibson and Crooks'. These concepts used 'tentacle-like' algorithms that allowed for driving on straights and curves while negotiating obstacles (Von Hundelshausen et al., 2008; Hu et al., 2018). These algorithms generated the possible future paths originating from the current state of the vehicle (based on several different methods such as rapidly-exploring random trees (RRT) and trajectories of maximum lateral acceleration at different speeds) which resembled tentacles extending from the front of the vehicle. These algorithms scanned the driver's preview area and used that information for planning the path through the environment. Although these algorithms were not intended to be human-like, their success in navigating through several scenarios indicates that area-based models could potentially provide an understanding of human driving behavior in several scenarios (Kadar and Shaw, 2000).

As indicated above, the use of field-based approaches is promising in modeling human driving behavior and for using it in the controllers of automated vehicles. However, so far, there appears to be no experimental evidence as to whether such a field is perceived and used by humans while driving. In this study, we take a step towards operationalizing the field of safe travel (Gibson and Crooks, 1938) by measuring the 'Driver's Risk Field' (DRF): a quantification of the driver's steering response as a function of the region (area) in front of the vehicle. It is important to point out that the DRF defined in this study and the field of safe travel are two different concepts. To put it in the context of other literature, Näätänen and Summala (1976) suggest that a driver's perceived risk is the product of (i) the importance given by the driver to a hazardous event occurring and (ii) the consequences of the event. In this paper, we hold the second part (consequence of the event) constant by performing obstacle avoidance tasks with identical obstacles. We assume that when the drivers think that they may collide with the obstacle they respond proportionally to the perceived risk. With this assumption, the DRF represents the first part: the importance given by the driver to an obstacle appearing (hazardous event) in his/her preview. The DRF can be used to estimate the driver's perceived risk, which will be a function of the car and driver state. The optimal values of this estimated risk (with respect to the yaw rate, heading, speed, etc. apart from the position of the vehicle), when plotted as a function of the position of the vehicle in the environment, will result in Gibson and Crooks' field of safe travel. The field of safe travel can, hence, be seen as the solution space of a path planning problem, whereas the DRF can be viewed as a component that helps generate this solution space.

To determine the shape of the DRF, different positions in the preview of the driver needed to be probed. For this study, we chose an obstacle avoidance task on a straight road, where an obstacle appeared at a specific lateral and longitudinal location. The experiment was conducted in a driving simulator instead of in a real car, for safety and experimental control.

The shape of the DRF (2D projection on the road surface) was hypothesized to expand (i.e., widen) as the longitudinal distance from the vehicle increases (Fig. 1). This hypothesis was based on neurophysiological studies that have provided evidence for the presence of noise in the human sensors (vision, proprioception, etc.) and actuators (muscles) (Clamann, 1969). It is also known that humans try to minimize the effect of noise present in their sensorimotor control system (Harris and Wolpert, 1998; Wolpert and Landy, 2012). In the field of driving, it has been established that humans look ahead (preview) while driving (Land and Horwood, 1995). If predictions of positions of the vehicle are made, the noise/uncertainty will propagate and will result in an expanding region as the longitudinal distance increases (see Fig. 2 in Du et al., 2011).

Furthermore, we hypothesized that the height of the DRF decays as the lateral and longitudinal distance from the vehicle increase. This hypothesis is based on findings in the literature that show that with higher time margins, the response of the driver decreases. Jurecki and Stańczyk (2014) found that the driver became more relaxed (higher reaction times) as the risk of colliding with a pedestrian decreased (i.e., the time to collision (TTC) to pedestrians increased). Lewis-Evans et al. (2010) found that the perceived risk and task difficulty increased when the time headway during car following increased. In our study, we aimed to quantify these observations by finding the functions that describe these relationships.

2. Methods

2.1. Apparatus

Participants ($N = 8$) drove in a fixed-base simulator at the Control and Simulation Department at the faculty of Aerospace Engineering, Delft University of Technology. Self-aligning torques of the front wheels were provided by a MOOG FCS ECOl8000 S steering motor running at 2500 Hz. A single-track model (heavy sedan of 1.8 m width) was used to simulate the vehicle dynamics. The environment was shown using three digital light processing (DLP) projectors (BenQ W1080ST 1080p Full HD), together providing a horizontal and vertical field-of-view of 180° and 40°, respectively. The visuals were displayed with a frame rate of 60 Hz, and the data was logged at 100 Hz. The (front) bonnet/hood of the car was visualized to facilitate a more accurate perception of the car's position relative to the road boundaries (Fig. 2).

2.2. Participants

Since our goal was to examine functional relationships at the level of individual participants, it was decided to follow a design in which a large number of observations were made on a relatively small number of participants (Smith and Little, 2018). Eight participants (7 male, 1 female) with normal or corrected-to-normal vision volunteered for this study and performed 308 obstacle avoidance trials. Participants had the following characteristics (Mean ± SD) [units]: age (25.4 ± 1.7) [years], driving experience (6.1 ± 2.0) [years], driving frequency in the last 12 months (2.1 ± 1.8) [trips/week], and distance driven in the past 12 months (4712 ± 688) [km].

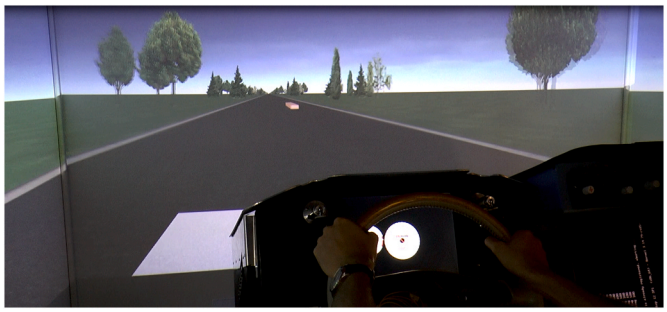

Fig. 2. A snapshot of the driving scene from the simulator, at the moment the obstacle appeared in front of the driver. The participants drove a 1.8 m wide car on a 7 m wide road with no center lane markings, at a constant speed of 25 m/s.

2.3. Experimental setup

Participants had to avoid an obstacle that appeared at one (randomly chosen) of the 77 positions.[1] Each obstacle position was encountered 4 times, once per block of 77 trials. In total, each participant performed 308 obstacle avoidance trials. The experiment was spread out over two separate (not necessarily consecutive) days, with each day consisting of 2 blocks of approximately 30 min each. Each block consisted of 3 sub-blocks of approximately 8 min each. Sub-blocks 1, 2, and 3 consisted of 26, 26, and 25 trials, respectively, which resulted in each block making up 1 repetition of 77 trials. The trials were randomly ordered among the sub-blocks to ensure that participants could not anticipate the position of the obstacles.

2.4. Road and obstacle design

2.4.1. Road design

Participants drove on a straight single-lane 7 m wide road, with no center lane markings, and no traffic. The road was designed to be wide, to minimize the cues that participants would get from the lane boundaries with respect to the obstacle positions.

2.4.2. Obstacle positions

The 77 obstacle positions formed a grid that was used to determine the shape of the DRA. There were 7 columns of obstacle positions, and each column consisted of 11 positions. The distances were calculated from the center of the obstacle to the center of the vehicle, with longitudinal and lateral directions being parallel and perpendicular to the heading of the road, respectively. The 7 columns were at longitudinal distances of 25 m, 50 m, 75 m, 100 m, 125 m, 150 m, and 175 m in front of the vehicle center. In each of the columns, the obstacles were positioned at lateral distances of 2.05 m, 1.85 m, 1.65 m, 1.45 m, 1.25 m, 0 m, −1.25 m, −1.45 m, −1.65 m, −1.85 m, and −2.05 m, from the lane center. A positive value indicates that the obstacle was to the left of the lane center, negative to the right, and zero indicates that the obstacle was on the lane center.

As can be noticed, the 5 obstacles to the left and right of the lane center were laterally positioned 20 cm apart, but the distance between the obstacle at ± 1.25 m and the obstacle at 0 m was 1.25 m. The vehicle used in the simulator was 1.8 m wide, and hence, any obstacle positioned within 1.025 m (1.8/2 + 0.25/2) of the lane center would have to be always avoided. All the obstacles beyond 1.025 m, theoretically, did not need to be avoided, as they were beyond the width of the car. Accordingly, in our experiment, 70 out of 77 obstacles (i.e., all obstacles except the 7 in the center row) did not have to be avoided. The participants were not made aware of this information.

2.4.3. Obstacle properties

Each obstacle was a cuboid with a rectangular cross-section (height x width = 12.5 cm × 25 cm) and length of 15 m. The obstacle laid flat on the road with its long axis parallel to the road heading. The obstacle was relatively long to encourage participants not to steer back immediately after they have passed the front of the obstacle.

2.4.4. Driving task

The experiment was conducted at a constant vehicle speed (25 m/s), since the intention was to measure the response of the driver solely by means of steering. If speed control were handed over to the driver, it could be expected that the response of the driver would get distributed over steering and speed control. Additionally, it was necessary to ensure that, in every trial, the relative distance between the vehicle and the obstacle is realized, as per the design (Fig. 3). Therefore, guidance torques were exerted on the steering wheel, which guided the vehicle to the lane center, before the start of each trial. A small buzzing vibration was also added to the steering wheel to convey to the driver that the vehicle is guiding itself to the lane center.

Each trial was assigned a road section of 350 m, and the obstacle appeared at the start of this section (Fig. 4). As soon as the obstacle appeared, the lane centering guidance was deactivated. The driver then performed the maneuver, and 50 m after the obstacle center had been passed by the vehicle center, the guidance torques would come into effect. As soon as the next obstacle appeared, the guidance torques were deactivated, and the experiment continued with the subsequent trial.

Because the obstacles appeared at random positions and the lane centering guidance system took over after the obstacle was passed, the duration for which the guidance system was on was also random. This random duration mitigated the problem of participants anticipating the obstacle appearance based on the duration for which the guidance was on.

2.5. Measuring the driver's response

Whether the DRF is subjective (only perceived) or objective (visible in the driver's actions) is an important point that needs to be investigated. If the DRF is subjective but not objective, then it could be a quirk of human perception, where people subjectively experience the DRF but do not act accordingly. Conversely, if it is objective but not subjective, then apparently people perform their steering actions subconsciously, without necessarily being aware of what they are doing. These, however, are extreme cases. Different shapes of DRF for subjective and objective steering responses could provide insights into the driver's awareness and perception of the driving scene. Thus, the experiment measured both the subjective and the objective steering responses of the participants during an obstacle avoidance task, and the results are analyzed independently without assuming any dependency of one on the other.

2.5.1. Objective response

The objective measure was calculated as the maximum of the absolute value of the steering angle applied from the instant the obstacle

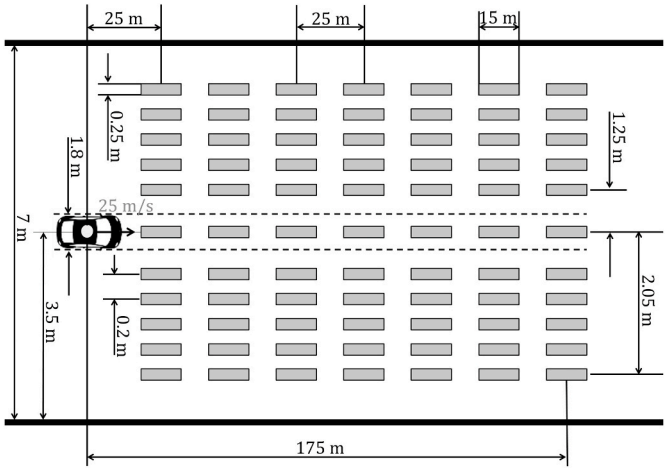

Fig. 3. The representation (not to scale) of the grid of obstacle positions. During each trial, an obstacle would appear at one of these 77 positions (11 lateral and 7 longitudinal positions). If driven straight, only the center row of obstacles obstructed the vehicle. All other obstacles were at a lateral distance (at least 0.225 m) greater than the width of the car.

[1] In the experiment we had 78 obstacle positions, but the 78th position was not used for analysis in this study. It appeared as the 26th obstacle of every Sub-block 3 and was positioned on the lane center (lateral position = 0 m) at a longitudinal distance of 350 m. This obstacle was implemented for analysis which will be performed in a follow up study, and has not been considered for analysis in this study.

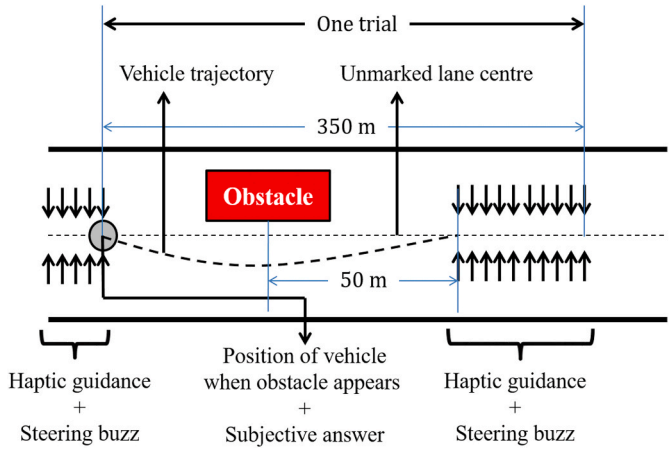

Fig. 4. A trial started when the obstacle appeared. The participant was expected to provide a numerical value (subjective response) and perform (or not perform) a steering maneuver to avoid the obstacle. Fifty meters after the vehicle center had passed the obstacle center, the lane centering guidance forces took over and guided the participant to the lane center, in preparation for the next trial. The guidance deactivated, as soon as the next obstacle appeared, which also marked the beginning of the next trial.

appears to the point when the vehicle center travels 25 m (1 s, since the speed of the vehicle = 25 m/s). In Fig. 5, this is indicated from 0 m longitudinal distance until the dotted vertical line. This ensured that we captured the initial response of the participants since we were interested in quantifying the shape of the DRF at the "current instant in time".

2.5.2. Subjective response

For each trial, participants had to say aloud a non-negative real number as soon as the obstacle appeared. The number was an answer to the question: "How much steering do you think you need, at this moment?". The words "at this moment" are an important part of the question, since the DRF, as previously defined, relates to the perceived risk at the current time instant. Participants were instructed to report zero if they did not feel the need to steer at the current time instant. The question was stated at the beginning of the experiment (on each day) and was not repeated for each trial. The participants were expected to respond as soon as the obstacle appeared. They were trained for this with a 6 min trial at the start of each day. No scale or reference values related to the subjective response were provided to the participants (Stevens, 1975). This approach was used to prevent the saturation of

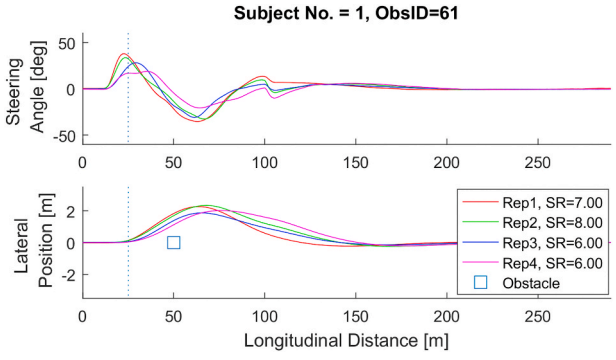

Fig. 5. The figure shows the steering angle applied by a participant and the lateral position of the vehicle on the road as a function of the longitudinal distance along the lane center. In this particular example, the obstacle appeared on the lane center (lateral position 0 m) at a longitudinal distance of 50 m. The four lines represent the four repetitions for this particular obstacle position (Rep1 = first repetition). SR = subjective response of the participant for the corresponding trial.

subjective answers towards the extremes of a predefined scale, which is important in our experiment because the participants did not know the lowest or highest level of stimulus beforehand. Also, this approach provided more freedom to the participants, as it did not require them to multiply, divide, etcetera to scale their responses to the given reference value (Stevens, 1975, p 28).

3. Analyses

In this paper, the analysis and results are reported for each participant independently. For each trial, we calculated a subjective and objective measure, as described in the methods section. Three-hundred-eight responses were recorded per participant for the subjective and objective measure, each. All participants were instructed to report a subjective response of '0' to indicate 'no steering needed at this instant in time'. A similar threshold that distinguishes between a 'steering action' and 'no steering action' is needed for the objective measure since the objective measure will never be exactly 0. A steering angle threshold of $\pm 2^{\circ}$ was used as a threshold for the objective measure since literature indicates that $\pm 2^{\circ}$ represents a conscious steering action (Johansson et al., 2004; Markkula and Engström, 2006; Petermeijer et al., 2017). This means that if the maximum of the absolute of the steering angle applied by the participant was less than 2°, the objective measure was set to 0, for that particular trial. Following this, for both subjective and objective measures, the 4 repetitions for the 77 obstacle locations were averaged and rearranged in an 11 x 7 matrix (11 lateral positions and 7 longitudinal positions). It is important to note that we performed the experiment at a constant speed and we expect speed to have a significant effect on the DRF (which will have to be quantified in future studies). Hence, to avoid the speed dependency, we report our results in terms of distances and not in terms of time-based measures such as time to collision (TTC) or time headway (THW).

3.1. Shape of the driver risk field (DRF)

We investigated the relationship between the position of the obstacle and the steering responses (subjective and objective), to determine the shape of the DRF, with respect to the 3 axes:

1) y-axis: Effect of the lateral position of the obstacle on steering response (subjective and objective)
2) x-axis: Effect of the longitudinal position of the obstacle on steering response (subjective and objective)
3) z-axis: Contours of steering response (subjective and objective)

For each of these 3 axes, the data was fit to a function (Gaussian, power curve, or parabolic), and the R^2 index was calculated to assess the goodness of fit for each fit. A nonlinear least-squares method with the Trust-Region algorithm was used to find the optimal parameters (Coleman and Li, 1996). The analysis is identical for subjective and objective steering response and performed for each participant independently.

3.1.1. Effect of the lateral position of the obstacle on steering response

The effect of lateral position on the steering response was studied by using the 11 data points per longitudinal position (Fig. 6, Row 1). Each row of 11 data points (in cutting planes parallel to the y-z plane) was used to fit a Gaussian function (1).

$$z = a_1 \, e^{\frac{-y^2}{a_2^2}} \tag{1}$$

where a_1 and a_2 are the parameters to be estimated. The steering responses had their maximum value at the lane center and decayed to zero on either side of the lane center, for each of the 7 longitudinal positions. Accordingly, the continuous and differentiable Gaussian function was chosen over other simple functions such as linear functions or parabolas. The R^2 index was calculated per participant by taking a mean of the R^2

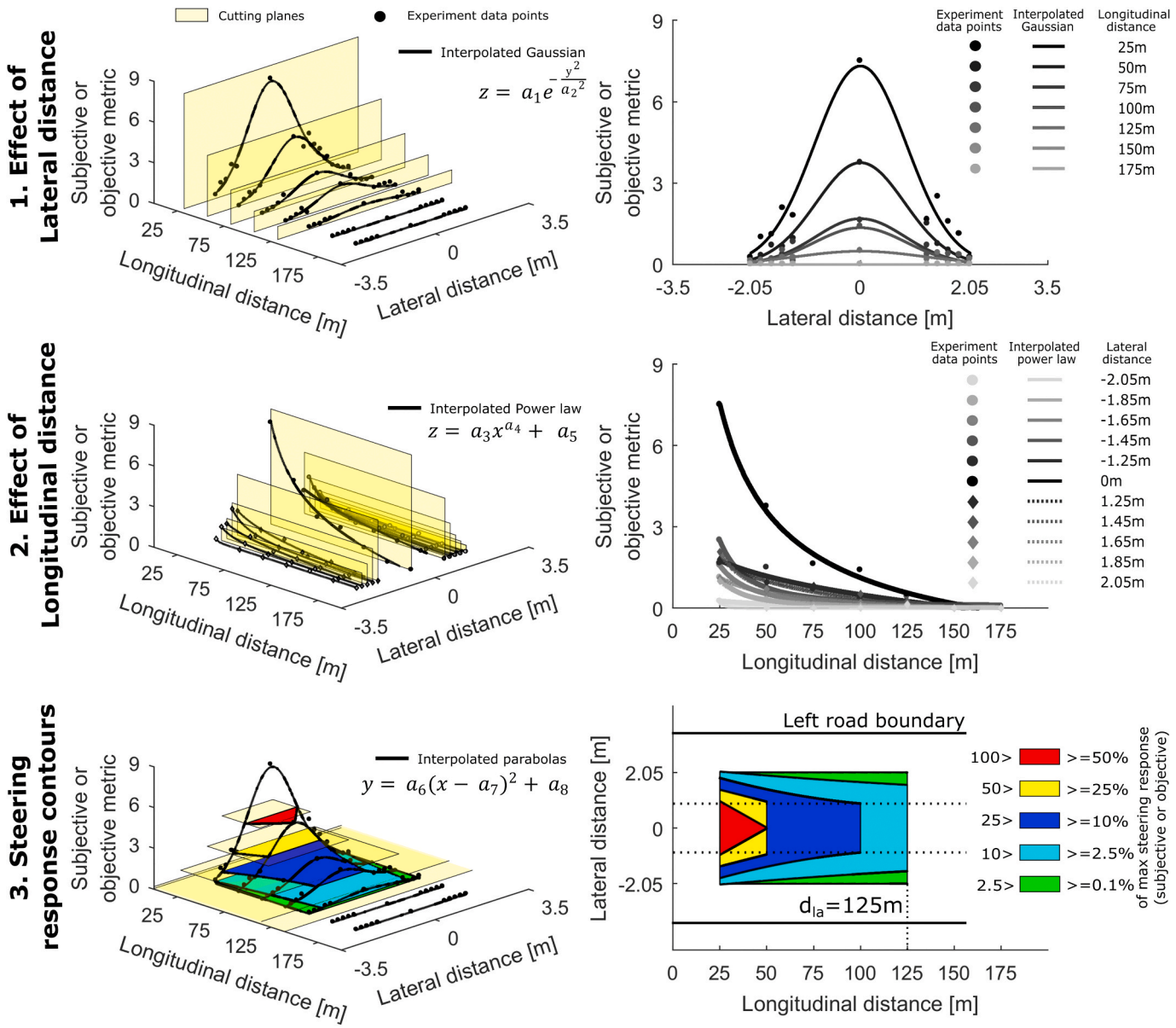

Fig. 6. Shape of the DRF was analyzed along the y (lateral obstacle position) and x (longitudinal obstacle position) axes. The left column illustrates the analysis performed on the experimental data (black circles) using the (pale yellow) cutting planes to arrive at the results shown in the right column. The look-ahead distance (d_{la}) was the distance along the longitudinal axis, beyond which the steering response of the driver was 0. (For interpretation of the references to colour in this figure legend, the reader is referred to the Web version of this article.)

index of each of the 7 (longitudinal positions) curves.

3.1.2. *Effect of longitudinal position on of the obstacle on steering response*

The effect of longitudinal position on the steering response was studied by using the 7 data points per lateral position (Fig. 6, Row 2). Each column of 7 data points was then used to fit a power function (2).

$$z = a_3\, x^{a_4} + a_5 \tag{2}$$

where a_3, a_4, and a_5 are the parameters to be estimated. A power curve was fit to the experimental data because, from visual inspection, it could be seen that the steering response decays as the longitudinal position increases, an effect that bears a resemblance to the relationship between an objective stimulus and a subjective response studied by Stevens (1975). The R^2 index is calculated, per participant, by taking a mean of the R^2 of each of the 11 (lateral positions) curves.

3.1.3. *Shape of contours representing constant steering responses*

The interpolated Gaussian functions (previous subsection) are 'sliced' (parallel to the x-y plane) at 5 levels of steering response (0.1%, 2.5%, 10%, 25%, 50% of the maximum value of the measure). The max value is calculated per participant, separately for the subjective and objective measure. The points at which these cutting planes intersect the interpolated Gaussians are calculated and used to fit a second-order polynomial (3)

$$y = a_6(x - a_7)^2 + a_8 \tag{3}$$

where a_6, a_7, and a_8 are the parameters to be estimated and x is the longitudinal distance.

A parabolic function was chosen because it is the lowest degree of the polynomial capable of estimating curvature. The number of data points available for curve fitting was a factor of consideration because we probed seven longitudinal distances (25 m–175 m), but participants

could have lower look-ahead distances (d_{la}), resulting in a smaller (than 7) number of data points available for interpolation. Hence, a polynomial of the second order was chosen. If the cutting plane intersected only two Gaussians, then linear interpolation (4) was used because interpolating a parabola is not feasible with less than three points.

$$y = a_6\, x + a_7 \tag{4}$$

If the cutting plane intersected less than two Gaussians, a region could not be calculated, and hence is not shown in the plots. The R^2 index was calculated per participant by averaging the R^2 index of each curve. There are five cutting planes and each plane results in two boundary curves (left and right), which are mirror images of each other about the longitudinal distance (x) axis since the Gaussian function is centered at a lateral position of 0 (1).

3.2. Width of the Gaussian cross-section along longitudinal distance

In the previous subsection, we proposed to quantify the cross-section of the DRF with a Gaussian function the height of which decays as a power-law function of the longitudinal distance. However, the propagation of the width of the Gaussian function along the longitudinal distance is not quantified. For this, we fit a 2nd order polynomial to the a_2 parameter (Equation (1)) of the Gaussian function at each longitudinal distance.

$$\sigma = a_9(x - a_{10})^2 + a_{11} \tag{5}$$

The 3 parameters for (a_9, a_{10}, a_{11}) of the second-order polynomial (5) define the shape of the propagation of the width of the DRF along the longitudinal distance (x). Parameter a_9 dictates the curvature of the boundary ($a_9 > 0$, curves upwards and $a_9 < 0$, curves downwards). Parameter a_{10} defines the position along the longitudinal distance, at which the curve reaches its inflection point (slope = 0). Parameter a_{10} can be classified into three regions: (i) $a_{10} < 25$ (in front of the near end), (ii) $25 < a_{10} < d_{la}$ (between the near and far end), and (iii) $a_{10} > d_{la}$ (beyond the far end). d_{la} is the look-ahead distance of a particular participant. If the obstacles appear beyond the d_{la}, the participant does not feel the need to steer immediately (Fig. 6). Parameter a_{11} defines the lateral position of the inflection point of the curve. Hence a_9 is classified in 2 ways ($a_{10} > 0$, $a_{10} < 0$), a_{10} is classified in 3 ways ($a_{10} < 25$, $25 < a_{10} < d_{la}$, $a_{10} > d_{la}$), and a_{11} is classified in 2 ways ($a_{11} > 0$, $a_{11} < 0$). Hence, there are 12 (2 x 3 x 2) possible shapes, 4 of which are shown in Fig. 7. The Type 1 shape resembles an hourglass, widening at the ends and narrowing in the middle. Type 2 looks like a funnel that widens from one end to the other, and Type 3 is 'opposite' of Type 2, where the funnel narrows as the longitudinal distance increases. Type 4 bulges outwards while narrowing from the near end to the far end. We plot the left boundary using (5) ($a_2 > 0$) and its 'mirror image' ($-a_2 < 0$) about the longitudinal axis to provide better visualization and understanding of the shape that would propagate (Fig. 7).

4. Results

4.1. Shape of the driver risk field (DRF)

4.1.1. Effect of the lateral position of the obstacles on the steering response

The effect of lateral position of the obstacles on the steering response of all eight participants (individually) is shown in Fig. 8 (subjective: top two rows, objective: bottom two rows). As hypothesized, the magnitude of steering response decreased as the lateral distance of the obstacle from the lane center increased (on either side). All participants responded to obstacles beyond the width of the car (±0.9 m), indicating that the area in the driver's preview that stimulates a steering correction is wider than the width of the vehicle and that drivers prefer to adopt a lateral safety margin to the obstacles.

Individual differences can be found in the height and width of the

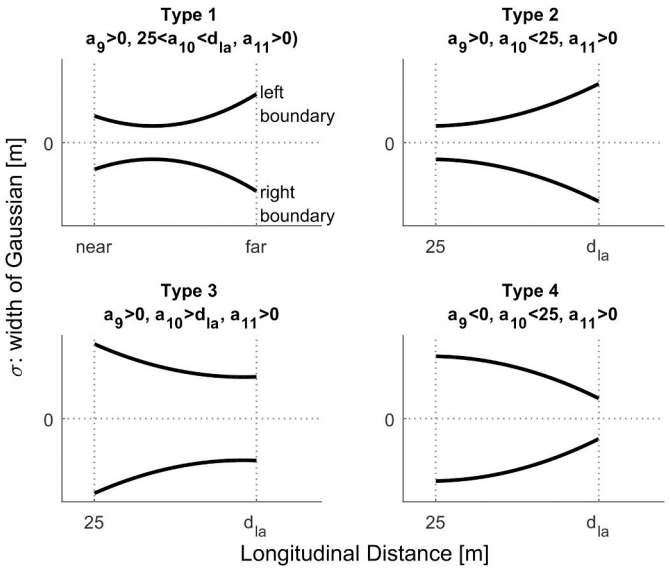

Fig. 7. Width of the Gaussian cross-section as a function of longitudinal distance: The three parameters (a_9, a_{10}, a_{11}) can form 12 different shapes, 4 of which are shown. The direction of travel of the vehicle is along the positive x-axis, and the near and far end are located at 25 m and d_{la} (look-ahead distance) in front of the vehicle, respectively.

Gaussians. For example, S1 and S5 have narrow Gaussians, whereas S4 and S8 have wide Gaussians. As the longitudinal distance of the obstacle to the vehicle increases, the magnitude of steering response decreases (as shown by the grayscale gradient lines in Fig. 8). The range of angles applied by the participants (objective measure) was quite similar (in the range of 0–80 deg), while the subjective responses had widely varying ranges. For example, S8 had a range from 0 to 100, while S3 had a range from 0 to 4. A Gaussian function accurately described the effect of lateral position on subjective ($R^2 = 0.77$) and objective ($R^2 = 0.69$) steering responses.

4.1.2. Effect of the longitudinal position of the obstacles on the steering response

The effect of the longitudinal position of the obstacles on the steering response is shown in Fig. 9 (subjective: top two rows, objective: bottom two rows). As the longitudinal distance of the obstacle from the vehicle increases, the magnitude of steering response decreases. Individual differences can be found in the height and the rate at which the responses decline as a function of longitudinal distance. For example, S3 and S7 have gradual rates of descent of steering response, whereas S5 and S6 have steep rates of descent. As the lateral distance to the lane center increases, the magnitude of steering response decreases (as shown by the grayscale gradient lines in Fig. 9). A power law was used to describe the effect of the longitudinal position of the obstacle, on subjective ($R^2 = 0.86$) and objective ($R^2 = 0.98$) steering responses.

4.1.3. Contours of constant steering responses

The results in Fig. 10 show the regions in the DRF that correspond to different intervals of steering response. The intervals were defined relative to the maximum steering response (subjective and objective) of each participant. There are clear individual differences in the way participants responded to obstacles. For example, S2 has a very wide DRF compared to S1. As the magnitude of steering response increases (0.1%–50%), the area of the corresponding contour region shrinks towards the vehicle. It is also evident that the participants used different look-ahead distances (d_{la}). Most participants (S1, S2, S4, S5, S6, S8) have the same look-ahead distance for subjective and objective measures.

Participants S3 and S7 have a shorter look-ahead distance calculated from the objective measure as compared to that calculated from the

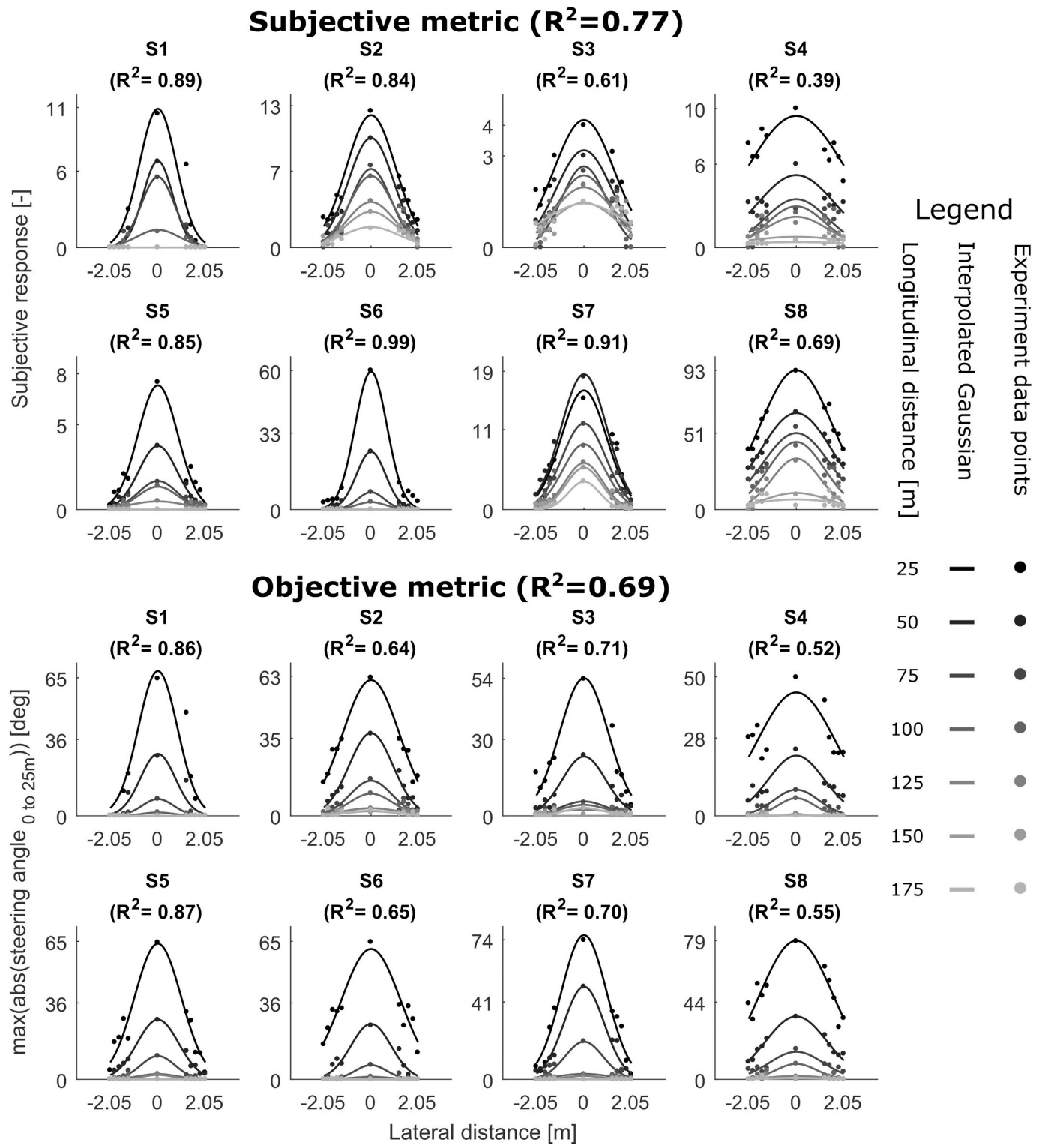

Fig. 8. The figure shows the effect of lateral distance (of the obstacle center from the lane center) on the steering response for the eight participants (S1–S8). The x-axis represents the lateral distance of the obstacle from the lane center (left of lane center is positive), and the y-axis represents the subjective response (top 2 rows) and the objective measure of max absolute steering angle (bottom 2 rows).

subjective measure. This means that participants consciously decided to make a correction, but the steering corrections were smaller than the 2 deg steering angle threshold that we set (to differentiate a conscious steering action from noise). Some of the subplots do not have the 50% (red) plane plotted (subjective: S6, objective: S1, S3, S4, S6, S8), since the 50% cutting plane intersected with less than two Gaussians.

4.2. Width of the Gaussian cross-section along longitudinal distance

The width of the Gaussian function (a_2) for each longitudinal distance was used to interpolate a parabola to determine the shape of the propagation on the DRF (Fig. 11). The 95% confidence interval of the estimation of a_2 is shown in grey markers.

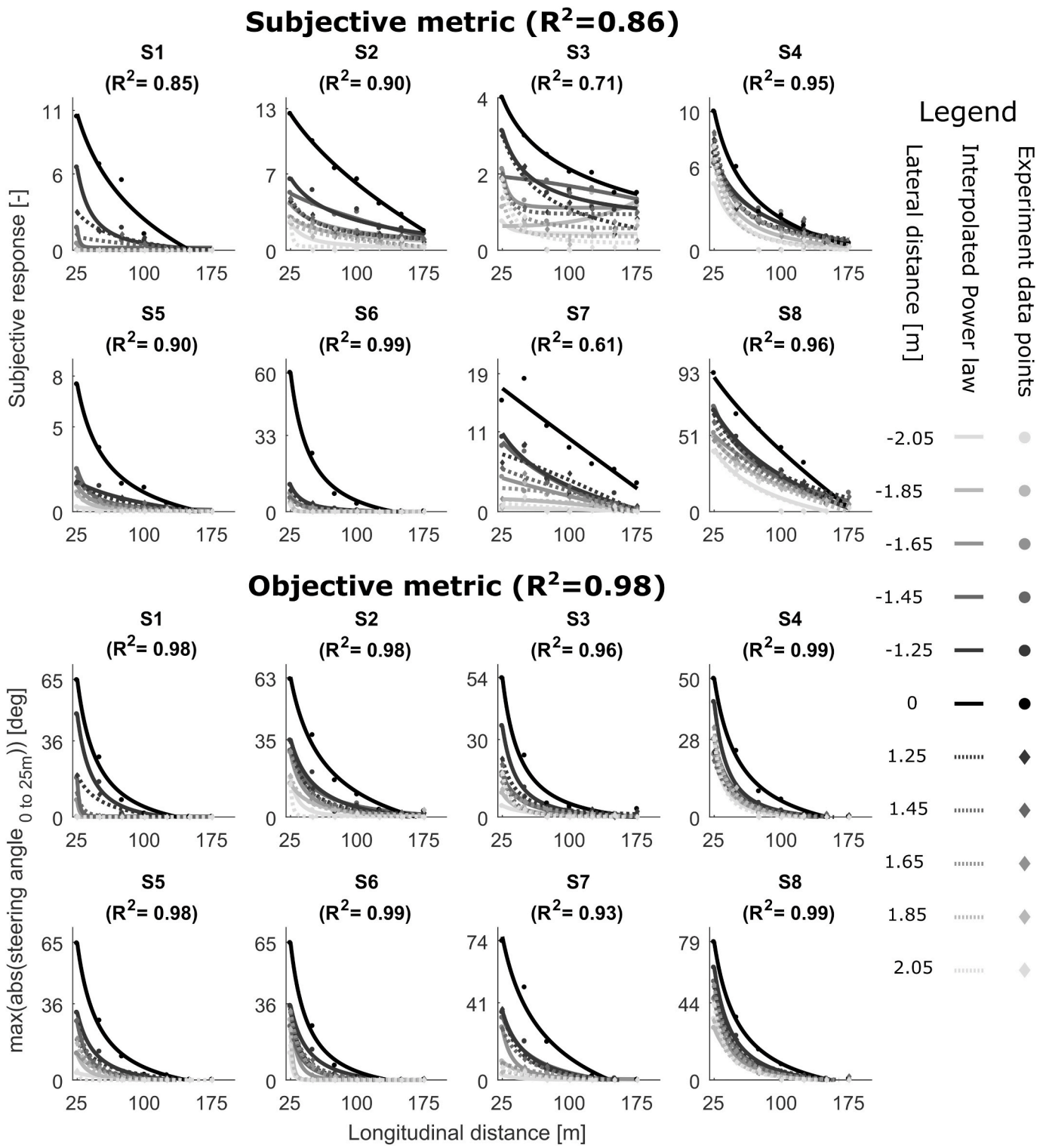

Fig. 9. The figure shows the effect of longitudinal distance (of the obstacle center from the vehicle center) on the steering response for the eight participants (S1-S8). The x-axis represents the longitudinal distance of the obstacle from the vehicle (the vehicle is traveling in the positive x-direction), and the y-axis represents the subjective response (top 2 rows) and the objective measure of max absolute steering angle (bottom 2 rows).

The shape was quantified by the parameters of the parabolic boundaries (a_9, a_{10}, and a_{11}) as explained in the analysis section (reported in Table 1: Supplementary material), and was classified into Type 1, 2, 3, or 4 (Fig. 7), according to the parameter values. The interpolated Gaussian functions with height (a1) = 0 were not used for fitting the parabolas since 0 steering response indicated 'no immediate steering required'. Most of the shapes (six of eight for subjective, and seven of eight for objective) resemble an hourglass shape (Type 1). Participants S1 and S3's objective measure narrows as the longitudinal distance increases and hence is classified as Type 3, whereas the subjective measure of S7 narrows (with a bulge) and hence is classified as Type 4.

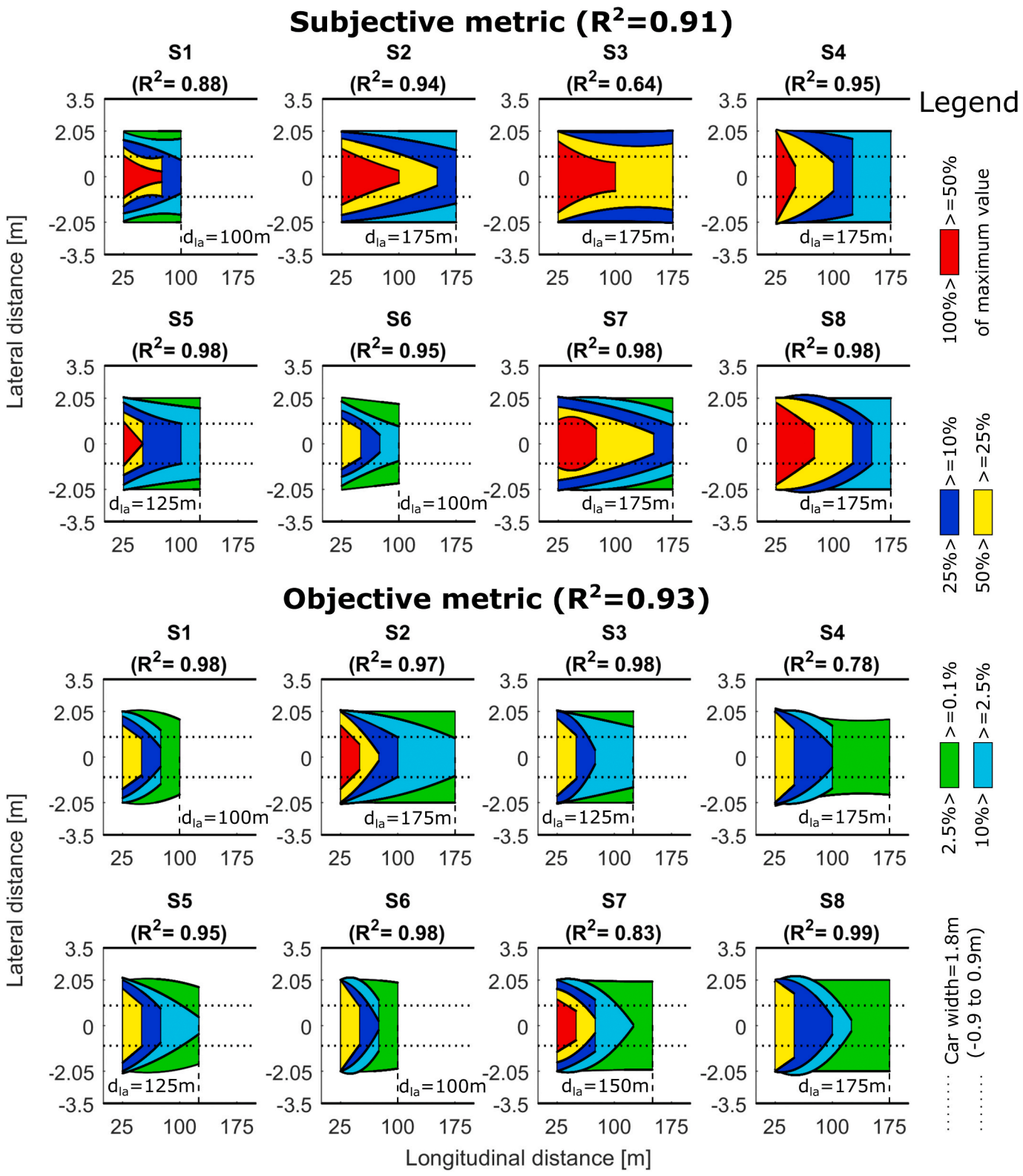

Fig. 10. The figure shows the regions of constant steering response at different intervals, for the eight participants (S1-S8). The different intervals (0.1%, 2.5%, 10%, 25%, 50%) are of the maximum value of the measure (subjective and objective, respectively), per participant. The x-axis represents the longitudinal distance of the obstacle from the vehicle (the vehicle is traveling in the positive x-direction), and the y-axis represents the lateral distance of the obstacle from the lane center. All participants exhibit a DRF that is wider than the width of the car (horizontal dotted lines).

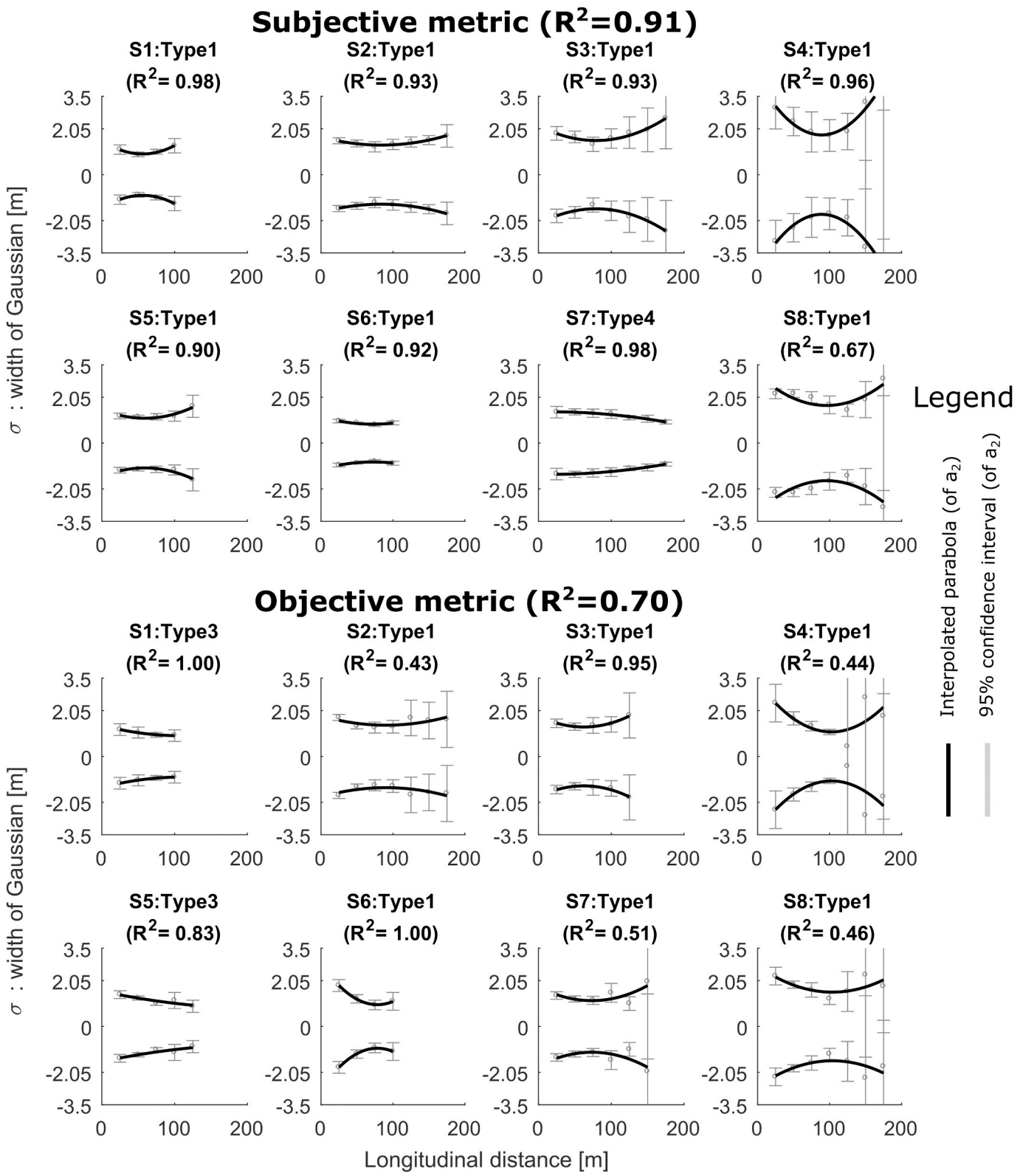

Fig. 11. The figure shows the effect of longitudinal distance on the width of the Gaussian cross-section of the DRF for the eight participants (S1-S8). The x-axis represents the longitudinal distance of the obstacle from the vehicle (the vehicle is traveling in the positive x-direction), and the y-axis represents the width of Gaussian. A parabolic function is fit to the width of Gaussian (parameter a_2 in equation (1)) at every longitudinal distance. The 95% confidence interval (calculated using the *confint* function in Matlab) are shown with the grey markers.

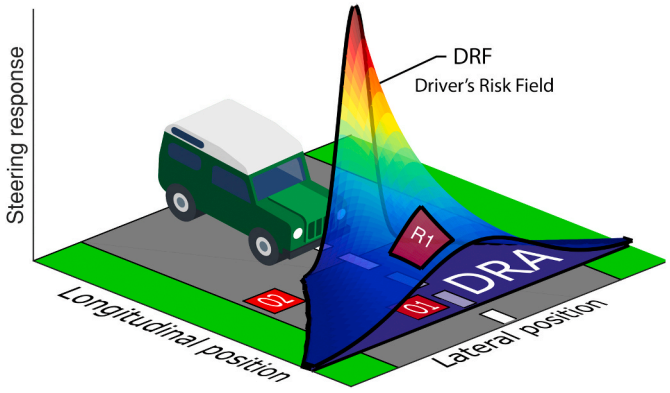

Fig. 1. Visualization of the hypothesized shape of the Driver's Risk Field (DRF). The height of the surface represents the magnitude of the steering response to an obstacle (subjective or objective). Obstacle O1 stimulates a response of magnitude R1, whereas obstacle O2 does not stimulate any response from the driver.

4.3. The relation between subjective and objective measures

When the subjective responses were compared against the corresponding objective responses, for each participant (Fig. 12), the Pearson correlation coefficients (r) indicated a strong association between them. This result shows that the DRF was not only perceived (subjective measure) but also acted upon (objective measure). However, there was a considerable number trials (especially for participant 4, $N_{obj0} = 30$) where participants reported a non-zero subjective response but did not perform a steering action within 1 s of the obstacle appearing. This effect can also be seen in Fig. 10, where the subjective contours (Fig. 10 top 2 rows) with higher values (red, yellow, deep-blue) cover larger areas of the DRF, compared to their area in the objective contours (Fig. 10 bottom 2 rows). This indicates that even if the participants perceive the risk at the current instant in time, they do not necessarily act immediately.

5. Discussion

This study aimed to experimentally investigate the shape of the 'Driver's Risk Field' (DRF) by quantifying the steering response in an obstacle avoidance task, at a constant speed. The results (Figs. 8 and 9) show that the effect of lateral and longitudinal position of the obstacle on steering response can be quantified by the Gaussian function and the power-law, respectively. Hence, the DRF constitutes a function (Fig. 13-Right) describing driver risk along the direction of movement of the vehicle, where risk decreases in lateral direction according to a Gaussian function, and according to the power law in the longitudinal direction. The top-down projection of the function visualizes the Driver's Risk Field projected around the vehicle, and the propagation of the width of the risk field follows an hourglass shape (for most participants).

We hypothesized that the shape of the DRF would expand as the longitudinal distance increased (Type 2 shape), but the results show that the DRF is shaped like an hourglass (Type 1 shape) for most of the participants (Fig. 11). The Type 1 and 2 shapes are both wide at the far end, but the hourglass shape (Type 1) that we observed for most subjects also widens at the near end. This widening at the near end could be due to startle, because of an obstacle appearing suddenly in front of the participant (Fig. 13-Left). This startle could initiate an open-loop steering action, without completely processing the position of the obstacle. This open-loop type of steering response in emergency scenarios was also observed in a previous study by Van Auken et al. (2011).

We hypothesized that the steering response would decrease as the distance between the obstacle and the vehicle increases. This hypothesis was confirmed by the results in Figs. 8 and 9. The decrease in steering response magnitude for increasing longitudinal distance to an obstacle corresponds to previous studies. For example, in Gold et al. (2013), the

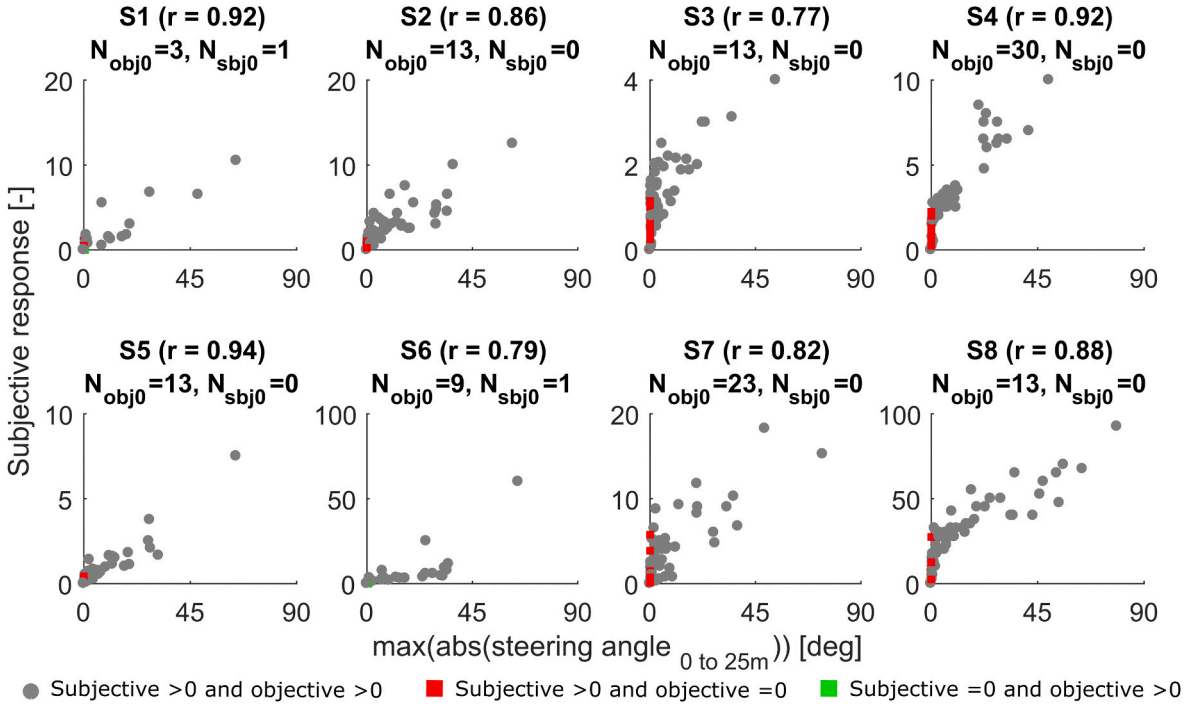

Fig. 12. The figure shows the correlation between the subjective response on the y-axis and the objective response (max of the absolute steering angle applied by the driver) on the x-axis. The Pearson correlation coefficient (r) is reported for each participant and indicates a high correlation between the subjective and objective measures (average of all participants: r = 0.86). N_{obj0} is the number of times (out of 77) that the objective measure was 0 and the subjective measure was non-zero (red squares), and N_{sbj0} is the number of times the subjective measure was 0 and the objective measure was non-zero (green squares). (For interpretation of the references to colour in this figure legend, the reader is referred to the Web version of this article.)

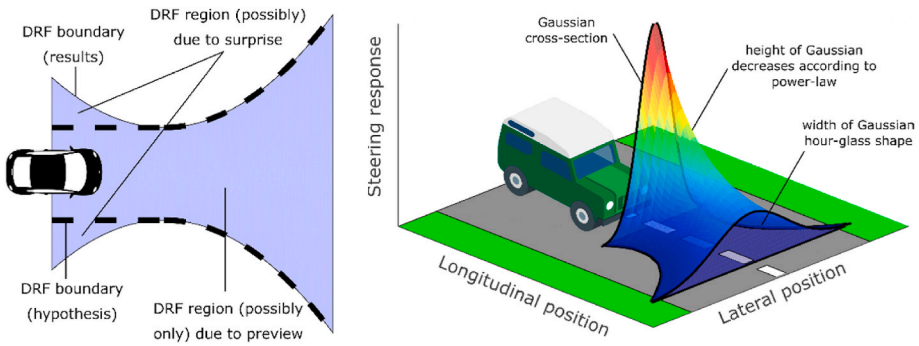

Fig. 13. (Left) The results of our study show that the DRF is hourglass-shaped (Type 1), whereas the hypothesis (marked by the dashed black lines) is funnel-shaped (Type 2). We argue that the widening towards the vehicle is due to the startle open-loop correction caused by an obstacle suddenly appearing at a short distance. (Right) Three-dimensional representation of the shape of the DRF. The height and width of the Gaussian cross-section follow the power law and the hourglass shape, respectively.

steering response (and hence the trajectory of the vehicle) became smoother as the take-over 'time budget' was increased (Fig. 4 in Gold et al., 2013). Other researchers found a decrease in subjective ratings of risk as the time headway (to a leading vehicle) increased, confirming our subjective results (Lewis-Evans et al., 2010; Siebert et al., 2014; Tscharn et al., 2018). An important contribution of our paper is that we captured this decrease in steering response as a function of increasing longitudinal distance by means of a power-law function for both subjective and objective steering response.

The shape of the DRF in this study is quantified at a constant speed. However, to fully understand the nature and properties of the DRF, experiments at different fixed vehicle speeds and with speed control handed over to the driver need to be carried out. The challenge here will be to derive a single DRF based on both lateral and longitudinal control since the driver's response is expected to be distributed over steering and braking/acceleration. We expect that the size of the DRF will scale with the speed of the vehicle, but maintain its shape. This prediction is based on the fact that drivers tend to maintain a constant look-ahead time, and hence the look-ahead distance, and in turn, the DRF scales with speed (Van Winsum and Heino, 1996).

The shape of the DRF, as quantified in this study, is based on the steering response magnitude as a function of the position of the obstacles. All the obstacles presented in this study were identical. This was done to study only the effect of the position of the obstacle and not its dangerousness. However, in the real world, obstacles pose different levels of risk. For example, a stone is less harmful than a rock (effect of size), a sheet of paper on the road is less dangerous than a pothole of the same size (effect of material), a static obstacle like road work equipment causes different response than dynamic obstacles such as pedestrians and vehicles (effect of speed). Future experiments should be done using obstacles posing different levels of hazard.

In this study, we measured the subjective and objective responses of the participants to examine if the risk field is perceived and/or acted upon. The results showed that the participants perceived (subjective response) and acted (objective response) on the risk. However, Fig. 12 showed that some participants perceived the risk at the current instant in time but did not act immediately. This means that sometimes the perceived risk is not large enough to elicit an immediate action (or any action at all). The relationship between the delay in responding to perceived risk and the position of the obstacle will be studied in the future.

One of the limitations of measuring subjective and objective response simultaneously is that there can be an interaction between the two responses. We tried to minimize this interaction by making the task 'subconscious' so that the participants did not consciously link their subjective and objective responses. We trained and motivated the participants to provide us their subjective response as soon as they saw the obstacle. Secondly, the participants could respond with any non-zero number and did not have to adhere to any predefined scale. This reduced the mental effort of consciously performing arithmetic calculations to provide a subjective response. Future studies could measure the subjective and objective measure separately and examine the interaction effect.

The DRF proposed in this study, which represents the importance given by the driver to a hazardous event occurring, can be combined with the 'consequences of the event' to calculate the perceived risk (Näätänen and Summala, 1976). This perceived risk could be used as a novel 'cost function' in controllers of automated driving/assistance systems. Fajen et al. (2003) performed a similar study with participants walking in an area strewn with obstacles and reported that such a field-based approach could predict the participant's path. The 'tentacle-like' algorithms in the field of robotics make use of the information from a vehicle's preview and show resemblance to the DRF. These similarities and the success of the area-based approaches in the field of robotics to negotiate a variety of scenarios indicates that the DRF can potentially be useful in several curve negotiation and obstacle avoidance scenarios (Chu et al., 2012; Von Hundelshausen et al., 2008; Hu et al., 2018; Werling et al., 2010). However, the main difference between the existing algorithms and the present DRF is that the former are derived from a control-theoretic point of view, whereas the DRF, as shown in this study, is perceived and acted upon by humans. We expect that our human-factors based approach can serve to improve the anthropomorphism of automated vehicles.

In recent years, 'human-like' driver models (Kolekar et al., 2017, Kolekar et al., 2018; Sentouh et al., 2009; Saleh et al., 2011; Benderius and Markkula, 2014) and personalized driver models that can describe and adapt to the behavior of individual drivers (Schnelle et al., 2016; Shi et al., 2015) have gained increasing attention. An important aspect of such models is the use of a function, the parameters of which can be modified to individualize driving behavior. The DRF in our experiment had an hourglass shape (for most participants), but its size was different for each tested individual. These individual differences can be captured by manipulating the parameter values and hence provide a means to individualize the DRF and make personalized driver models.

Note that in this study, we do not provide a unifying model or theory based on the quantified DRF. Such model development will have to be explored in future research, along with experimental studies to test the generalizability of the shape of the DRF for different driving scenarios. We hope that this paper thereby contributes to the development of automated vehicles that understand and interact with humans in a safer and more efficient manner.

6. Conclusions

In order to quantify the Driver's Risk Field (DRF) which is subjectively perceived and objectively acted upon by the drivers, we performed a driving simulator study where drivers needed to avoid suddenly appearing objects on a straight road at a constant speed. For the experimental conditions studied, we conclude the following:

1) Objective and subjective response of the drivers decreased as the lateral distance of the obstacle from the vehicle increased, and this

relationship could be described by the Gaussian function (Fig. 8: Subjective $R^2 = 0.77$, Objective $R^2 = 0.69$).
2) Objective and subjective response of the drivers decreased as the longitudinal distance of the obstacle from the vehicle increased, and this relationship could be described by the power-law (Fig. 9: Subjective $R^2 = 0.86$, Objective $R^2 = 0.98$).
3) All participants responded to obstacles that were placed beyond the width of the car, meaning that the quantified DRF exceeds car width. (Fig. 10).
4) For most of the participants, the propagation of the width of the DRF along the longitudinal distance resembled an hourglass shape (Fig. 11).

Declaration of competing interest

The authors declare no competing interests.

Acknowledgments

The Dutch Research Council (NWO) - The Netherlands, funded this project. Sarvesh Kolekar and David Abbink were supported by the VIDI 14127 project, and Joost De Winter was supported by the VIDI 178047 project. We also appreciate the valuable feedback provided by S. M. Petermeijer.

Appendix A. Supplementary data

Supplementary data to this article can be found online at https://doi.org/10.1016/j.apergo.2020.103196.

Author contributions

S.K. conceived the study; S.K. piloted the study and collected the data; S.K., J.d.W., D.A. conceived the analysis; S.K. analyzed the data; S. K. prepared the figures; S.K., J.d.W., D.A. wrote the manuscript.

Data availability

http://doi.org/10.4121/uuid:921b56a0-7ae0-4d5e-a8a1-bda219a00048

References

Abbink, D.A., Mulder, M., Boer, E.R., 2012. Haptic shared control: smoothly shifting control authority? Cognit. Technol. Work 14 (1), 19–28.
Benderius, O., Markkula, G., 2014. Evidence for a fundamental property of steering. In: Proceedings of the Human Factors and Ergonomics Society Annual Meeting, 58. SAGE Publications, Sage CA: Los Angeles, CA. No. 1.
Boer, E.R., 2016. Satisficing curve negotiation: explaining drivers' situated lateral position variability. IFAC-PapersOnLine 49 (19), 183–188.
Chu, K., Lee, M., Sunwoo, M., 2012. Local path planning for off-road autonomous driving with avoidance of static obstacles. IEEE Trans. Intell. Transport. Syst. 13 (4), 1599–1616.
Clamann, H.P., 1969. Statistical analysis of motor unit firing patterns in a human skeletal muscle. Biophys. J. 9 (10), 1233–1251.
Coleman, T.F., Li, Y., 1996. An interior trust region approach for nonlinear minimization subject to bounds. SIAM J. Optim. 6 (2), 418–445.
Denton, G.G., 1980. The influence of visual pattern on perceived speed. Perception 9 (4), 393–402.
Du, T., Noel, E., Burdick, J.W., 2011. Robot motion planning in dynamic, uncertain environments. IEEE Trans Robotics 28 (1), 101–115.
Fajen, B.R., Warren, W.H., Temizer, S., Kaelbling, L.P., 2003. A dynamical model of visually-guided steering, obstacle avoidance, and route selection. Int. J. Comput. Vis. 54 (1–3), 13–34.
Godthelp, H., Paul, M., Gerard, J.B., 1984. The development of a time-related measure to describe driving strategy. Hum. Factors 26 (3), 257–268.
Faltaous, S., Baumann, M., Schneegass, S., Chuang, L.L., 2018. Design Guidelines for Reliability Communication in Autonomous Vehicles. In: Proceedings of the 10th International Conference on Automotive User Interfaces and Interactive Vehicular Applications (September 2018), pp. 258–267.
Gibson, J.J., Crooks, L.E., 1938. A theoretical field-analysis of automobile-driving. Am. J. Psychol. 51 (3), 453–471.
Godthelp, H., 1986. Vehicle control during curve driving. Hum. Factors 28 (2), 211–221.
Gold, C., Damböck, D., Lorenz, L., Bengler, K., 2013, September. "Take over!" How long does it take to get the driver back into the loop?. In: Proceedings of the Human Factors and Ergonomics Society Annual Meeting, vol. 57 SAGE Publications, Sage CA: Los Angeles, CA, pp. 1938–1942. No. 1.
Harris, C.M., Wolpert, D.M., 1998. Signal-dependent noise determines motor planning. Nature 394 (6695), 780.
Hu, X., Chen, L., Tang, B., Cao, D., He, H., 2018. Dynamic path planning for autonomous driving on various roads with avoidance of static and moving obstacles. Mech. Syst. Signal Process. 100, 482–500.
Johansson, E., Engström, J., Cherri, C., Nodari, E., Toffetti, A., Schindhelm, R., Gelau, C., 2004. Review of Existing Techniques and Metrics for IVIS and ADAS Assessment (AIDE IST-1-507674-IP). Information Society, Brussels, Belgium.
Jurecki, R.S., Stańczyk, T.L., 2014. Driver reaction time to lateral entering pedestrian in a simulated crash traffic situation. Transport. Res. F Traffic Psychol. Behav. 27, 22–36.
Kadar, E.E., Shaw, R.E., 2000. Toward an ecological field theory of perceptual control of locomotion. Ecol. Psychol. 12 (2), 141–180.
Kauffmann, N., Winkler, F., Naujoks, F., Vollrath, M., 2018. "What Makes a Cooperative Driver?" Identifying parameters of implicit and explicit forms of communication in a lane change scenario. Transport. Res. F Traffic Psychol. Behav. 58, 1031–1042.
Kolekar, S.B., de Winter, J.C.F., Abbink, D.A., 2017. A human-like steering model: sensitive to uncertainty in the environment. In: 2017 IEEE International Conference on Systems, Man, and Cybernetics (SMC). IEEE, pp. 1487–1492.
Kolekar, Sarvesh, Mugge, Winfred, Abbink, David, 2018. Modeling intradriver steering variability based on sensorimotor control theories. IEEE Trans Human-Machine Sys 48 (3), 291–303.
Land, M., Horwood, J., 1995. Which parts of the road guide steering? Nature 377 (6547), 339–340.
Lappi, O., Mole, C.D., 2018. Visuomotor control, eye movements, and steering: a unified approach for incorporating feedback, feedforward, and internal models. Psychol. Bull. 144 (10), 981.
Lee, D.N., 1976. A theory of visual control of braking based on information about time-to-collision. Perception 5 (4), 437–459.
Lewis-Evans, B., Dick De, W., Brookhuis, K.A., 2010. That's close enough—a threshold effect of time headway on the experience of risk, task difficulty, effort, and comfort. Accid. Anal. Prev. 42 (6), 1926–1933.
Markkula, G., Engström, J., 2006. A steering wheel reversal rate metric for assessing effects of visual and cognitive secondary task load. In: Proceedings of the 13th ITS World Congress. Leeds.
McKnight, A.J., Adams, B.B., 1970. Driver education task analysis. Task Descriptions 1.
Melman, T., Abbink, D.A., van Paassen, M.M., Boer, E.R., de Winter, J.C.F., 2018. What determines drivers' speed? A replication of three behavioural adaptation experiments in a single driving simulator study. Ergonomics 61 (7), 966–987.
Muslim, H., Itoh, M., 2018. A theoretical framework for designing human-centered automotive automation systems. Cognit. Technol. Work 1–13.
Näätänen, R., Summala, H., 1976. Road-user Behaviour and Traffic Accidents. Publication of: North-Holland Publishing Company.
Neumann, P.G., 2016. Automated car woes—whoa there! Ubiquity 1. July (2016).
Niu, D., Terken, J., Berry, E., 2018. Anthropomorphizing information to enhance trust in autonomous vehicles. In: Human Factors and Ergonomics in Manufacturing & Service Industries, pp. 352–359.
Papakostopoulos, V., Marmaras, N., Nathanael, D., 2017. The "field of safe travel" revisited: interpreting driving behaviour performance through a holistic approach. Transport Rev. 37 (6), 695–714.
Petermeijer, S.M., Bazilinskyy, P., Bengler, K., De Winter, J.C.F., 2017. Take-over again: investigating multimodal and directional TORs to get the driver back into the loop. Appl. Ergon. 62, 204–215.
Rasekhipour, Y., 2017. Prioritized Obstacle Avoidance in Motion Planning of Autonomous Vehicles. PhD Thesis. University of Waterloo.
Reimer, B., 2014. Driver assistance systems and the transition to automated vehicles: a path to increase older adult safety and mobility? Public Pol Aging Report 24 (1), 27–31.
Saleh, L., Chevrel, P., Mars, F., Lafay, J.F., Claveau, F., 2011. Human-like cybernetic driver model for lane keeping. IFAC Proc Vol 44 (1), 4368–4373.
Schnelle, S., Wang, J., Su, H., Jagacinski, R., 2016. A driver steering model with personalized desired path generation. IEEE Trans Sys Man, and Cybernetics: Systems 47 (1), 111–120.
Sentouh, C., Chevrel, P., Mars, F., Claveau, F., 2009, October. A sensorimotor driver model for steering control. In: 2009 IEEE International Conference on Systems, Man and Cybernetics. IEEE, pp. 2462–2467.
Shi, B., Xu, L., Hu, J., Tang, Y., Jiang, H., Meng, W., Liu, H., 2015. Evaluating driving styles by normalizing driving behavior based on personalized driver modeling. IEEE Trans Sys Man, and Cybernetics: Systems 45 (12), 1502–1508.
Siebert, F.W., Oehl, M., Pfister, H., 2014. The influence of time headway on subjective driver states in adaptive cruise control. Transport. Res. F Traffic Psychol. Behav. 25, 65–73.
Smith, K., Källhammer, J., 2012. Experimental evidence for the field of safe travel. In: Proceedings of the Human Factors and Ergonomics Society Annual Meeting, 56. Sage Publications, Sage CA: Los Angeles, CA. No. 1.
Smith, P., Little, D., 2018. Small is beautiful: in defense of the small-N design. Psychon. Bull. Rev. 1–19.
Stevens, S.S., 1975. Psychophysics. In: Introduction to its Perceptual, Neural and Social Prospects. Routledge.
Tscharn, R., Naujoks, F., Neukum, A., 2018. The perceived criticality of different time headways is depending on velocity. Transport. Res. F Traffic Psychol. Behav. 58, 1043–1052.

Van Auken, R.M., Zellner, J.W., Chiang, D.P., Kelly, J., Silberling, J.Y., Dai, R., et al., 2011. Advanced Crash Avoidance Technologies Program–Final Report of the Honda-DRI Team, Volume II. Transportation Research Board. Appendix A through J (No. HS-811 454B).

Van Winsum, W., Heino, A., 1996. Choice of time-headway in car-following and the role of time-to-collision information in braking. Ergonomics 39 (4), 579–592.

Von Hundelshausen, F., Himmelsbach, M., Hecker, F., Mueller, A., Wuensche, H.J., 2008. Driving with tentacles: integral structures for sensing and motion. J. Field Robot. 25 (9), 640–673.

Werling, M., Ziegler, J., Kammel, S., Thrun, S., 2010, May. Optimal trajectory generation for dynamic street scenarios in a frenet frame. In: 2010 IEEE International Conference on Robotics and Automation. IEEE, pp. 987–993.

Wolpert, D.M., Landy, M.S., 2012. Motor control is decision-making. Curr. Opin. Neurobiol. 22 (6), 996–1003.